Phase locking in Josephson ladders and the discrete sine-Gordon equation: The effects of boundary conditions and current-induced magnetic fields

B. R. Trees and R. A. Murgescu
Department of Physics and Astronomy, Ohio Wesleyan University, Delaware, Ohio 43015
(Received 26 January 2001; published 20 September 2001)

We report on the stability of phase-locked solutions to ladder arrays of underdamped Josephson junctions under both periodic and open boundary conditions and in the presence of current-induced magnetic fields. We calculate the Floquet exponents based on the resistively and capacitively shunted junction (RCSJ) model, as well as on a simplified model of the ladder that leads to a discrete sine-Gordon (DSG) equation for the horizontal, current-biased junctions. In the case of zero induced magnetic fields, we find the DSG equation (commonly applied to parallel arrays) appreciably overestimates the exponents of the full ladder in the overdamped regime (corresponding to the limit of small junction capacitance, β_c), and that difference physically results from differing spectra for small-amplitude phase oscillations of the DSG and RCSJ equations. mutual inductance between plaquettes is included we find there are ranges of values for the mutual inductance for which the ladder is in fact unstable. To understand the cause of the observed instabilities, it is crucial to consider the behavior of the vertical junctions.

DOI: 10.1103/PhysRevE.64.046205 PACS number(s): 05.45.Xt, 74.50.+r, 02.40.Xx

I. INTRODUCTION

Ladder arrays of Josephson junctions are intriguing systems for a wealth of reasons: they offer rich dynamical behavior, accessible to both theorists and experimentalists, in the field of coupled nonlinear oscillators [1–10] (with recent interest in the prediction and observation of discrete rotobreathers [11–15]); the possibility of phase locking a maximal subset of junctions suggests their use as microwave sources [16–19]; their complexity is between that of better understood one-dimensional serial and parallel arrays and full 2D arrays (e.g., square arrays), and thus they offer a nice link between the two geometries; and ladder arrays can, under circumstances that are partially understood, be modeled by the discrete sine-Gordon (DSG) equation [6,20–22], which is itself a source of research interest among many [23]. In this paper we study the stability of phase-locked junctions in underdamped ladder arrays biased with uniform dc bias currents greater than the critical currents of the junctions. This means a subset of the junctions will be described by a Josephson phase of the form $\phi = \omega t + f(t)$, where ω is an angular frequency dependent on the bias current and $f(t)$ is a (usually) small periodic correction. Such junctions are often described as being in the whirling mode, in which the analogy between an individual Josephson junction and a damped, driven pendulum experiencing a gravitational torque has been invoked. In the mechanical case, ϕ describes the angular displacement of the pendulum, and ω is the angular speed of its rotational motion.

We report on two aspects of phase locking in ladders: the effects of boundary conditions (periodic versus open) as well as the effects of current-induced magnetic fields on the stability of phase-locked solutions in the whirling regime. Also, in a refinement and continuation of work previously reported [21], we have attempted to elucidate further the conditions under which the ladder's behavior is well described by that of the DSG equation. We use Floquet theory (see Sec. II) as the main tool towards these ends.

The form of the DSG equation in which we are interested is often described as representing a system of damped, driven particles that are connected to their nearest neighbors by simple springs and that experience an external potential that is a sinusoidal function of position [24]. In such a situation the DSG equation is also known as a variation of the well-known Frenkel-Kontorova model [25], which was proposed in the study of dislocations in crystals. It is important to note that, because of the Hooke-like spring force in the DSG equation, the interparticle interactions are described by a *convex* potential energy function, i.e., $V(y) \propto y^2$, where y is the displacement between neighboring particles. A description of the classical dynamics of underdamped Josephson junctions, however, often turns to the resistively and capacitively shunted junction (RCSJ) model [26]. A key feature of this model is that it leads to an interaction term between neighboring horizontal junctions in a ladder array (see Fig. 1) that is a *sinusoidal* function of the difference in the Josephson phases of the junctions. That is, the RCSJ model contains ''interparticle'' interactions described by a *nonconvex* function, $V(\phi_{j+1}-\phi_j) \propto \cos(\phi_{j+1}-\phi_j)$, where ϕ_j is the Josephson phase for the jth horizontal junction. Despite this difference in the structure of the interaction terms between the DSG equation and the RCSJ model, it has been argued that the two should be dynamically equivalent in the limit of small spatial variations of the Josephson phase differences along the ladder [27], basically when $\phi_{j+1}-\phi_j \ll 1$ and $\cos(\phi_{j+1}-\phi_j) \approx 1-(\phi_{j+1}-\phi_j)^2$ [Refs. [6,20]]. Such a constraint on the phase differences is easily satisfied in the highly underdamped limit, corresponding to large McCumber parameters ($\beta_c = 2eI_cR^2C/\hbar$, where I_c, R, and C are a junction's critical current, resistance, and capacitance, respectively), and indeed much theoretical and experimental work comparing ladders and similar (but not identical) parallel arrays of junctions to the DSG equation was performed for $\beta_c \gtrsim 50$ [2,6,28–31]. Trees and Hussain [21] calculated the Floquet exponents for phase-locked ladders numerically for the RCSJ model and compared the results with an ana-

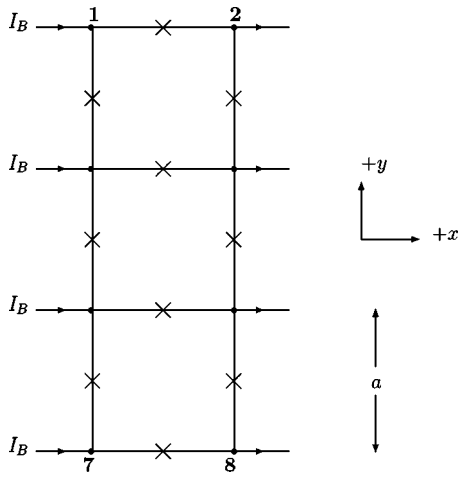

FIG. 1. Ladder array of Josephson junctions with cell size a. The horizontal junctions, along the rungs of the ladder, are parallel to the x axis, while the vertical junctions are parallel to the y axis. This figure depicts a ladder with $N=3$ cells and eight nodes, four of which are explicitly labeled. A dc bias current I_B is injected at each node on the left side and extracted from the right side. We assume either periodic or open boundary conditions along the long direction of the ladder.

lytic result obtained from the DSG equation for much smaller values of β_c, namely, $1<\beta_c\lesssim 50$. In comparing the Floquet exponents of smallest magnitude, which quantify the lifetime of the longest-lived perturbations to the array, they found excellent agreement between the two models down to McCumber parameters of approximately five (depending on ladder size). For even smaller β_c, the two results differed quantitatively, but qualitatively both showed a peak in the smallest exponent as a function of β_c [32].

The ladder geometry we have chosen to study is shown in Fig. 1. The junctions parallel to the x axis (the horizontal junctions) have a critical current I_{cx}, while the vertical junctions have a critical current I_{cy}. We have allowed for critical current anisotropy between the horizontal and vertical junctions so as to be able to tune the effective coupling between neighboring horizontal junctions (see Sec. II). For simplicity, however, all other junction parameters, e.g., resistance (R) and capacitance (C), are assumed identical. A possible refinement of this work would be to allow for resistive and capacitive disorder, while satisfying the constraint that the products I_cR and I_c/C for each junction be uniform throughout the array [33]. A spatially uniform, dc bias current I_B is fed into the horizontal junctions on the left and extracted from the right side. We typically allowed for a large dc bias of $I_B/I_c\approx 10$, thereby avoiding any instabilities between the whirling modes and the small-amplitude Josephson phase oscillations [29,30]. The long direction of the ladder (the y direction) experiences either periodic or open boundary conditions. The number of cells (plaquettes) of the ladder is denoted by N; typically we have studied ladders with N ranging from 5 to 25.

We consider phase-locked solutions for the horizontal junctions, by which we mean a solution in which the horizontal junctions have identical voltage versus time plots. In fact, if one initializes the superconducting phases and/or voltages at the nodes of the ladder randomly, it is easily determined from the numerical output of our code that the voltages, which are periodic in time, have indeed synchronized, i.e., phase locked, within a relatively few periods. To test the stability of phase-locking to mechanical perturbations, we calculate the Floquet exponents (see Sec. II) for these solutions. We do so both numerically for the RCSJ model, and analytically. Frequently, our analytic results are based on simplifying the dynamics of the full ladder to that of a DSG equation. For both the periodic and open ladders, *in the absence of induced magnetic fields*, we are able to obtain analytic results for the Floquet exponents directly from the RCSJ equations as well as from the DSG equation. We find these two analytic results agree well in the large β_c limit (underdamped regime), but differ substantially in the overdamped ($\beta_c\rightarrow 0$) regime. Furthermore, this difference is considerably more pronounced in the case of periodic ladders compared to open ladders (see Fig. 2). Physically, we find that differing spectra for small-amplitude phase oscillations between the two geometries accounts for this behavior.

We have also studied the effects of induced magnetic fields due to currents flowing in the plaquettes on the stability of phase-locked solutions. We do so in a controlled manner, first by considering only the self-inductance of a given plaquette. This enables us, in essence, to extend Fig. 2 and map out the minimum Floquet exponent as a function of junction capacitance *and* loop self-inductance (see Fig. 8). We are also able to calculate the exponents analytically based on the DSG equation, and we discuss the agreement between the numerical and analytical results in this case. We then include nearest-neighbor mutual inductance effects. Surprisingly, for a given ladder size, we find ranges of values for the mutual inductance over which the ladder exhibits unstable behavior, as evidenced by voltages and phases that grow exponentially with time. This is a geometrical effect, depending on the number of plaquettes and the size of the mutual inductance. Analytic work in this case, depending on both the DSG equation and the RCSJ equations, sheds light onto the cause of this instability. Last, we allow for long-range mutual inductance between plaquettes j and k, by allowing the strength of the mutual inductance to fall off exponentially with distance, i.e., we assume a mutual inductance of the form $M_{jk}=Me^{-s|j-k|}$, where distances are measured in units of the plaquette size a, and s tunes the range of the inductance. This is analogous to the inclusion of Kac-Baker long-range interactions in the DSG equation [23]. We still find the instability regions as for the case of nearest-neighbor inductance only, but even for those ranges of values of M for which phase locking still occurs, the degree of stability of that phase locking is *reduced* as the range of M_{jk} is *increased*, i.e., as $s\rightarrow 0$. In general, we find the inclusion of mutual inductance has a profound effect on the ability of horizontal junctions in the ladder to phase lock.

The remainder of this paper is organized as follows. In Sec. II we describe the numerical calculation of the Floquet exponents based on the RCSJ model and in the absence of induced magnetic fields. We also compare the effects of periodic versus open boundary conditions on the exponents. We

compare numerical results with two sets of analytic results, one based on the RCSJ equations for the full ladder and the other on a DSG equation. This comparison sheds light on the differing dynamics of the two models. In Sec. III we discuss the Floquet exponents in the presence of self-induced magnetic fields. In this case our numerical work is based on the RCSJ model, and our analytic work is based mainly on a DSG equation for the horizontal junctions. We discuss the degree to which the numerical and analytical results agree. In Sec. IV we also include the contribution to the induced magnetic field in a given plaquette due to currents flowing in neighboring plaquettes. It is at this point that we observe, for the first time in our work, unstable behavior, in which the Josephson phase differences across both the horizontal and vertical junctions grow exponentially with time. Section V discusses the effects of long-range mutual inductance, in which the induced magnetic field in a given plaquette is affected by currents flowing in all other plaquettes in the ladder. In Sec. VI we summarize our results.

II. BOUNDARY CONDITIONS/NO INDUCED FIELDS

A. RCSJ model

It is expedient to use a system of dimensionless variables. Let the characteristic time scale for a junction be $t_c \equiv \hbar/2eI_{cx}R$, so that we can define a dimensionless time variable, $\tau \equiv t/t_c$. The dimensionless dc bias current entering or leaving node j is $i_{B,j} \equiv I_{B,j}/I_{cx}$, where we are assuming uniform bias currents. Referring to Fig. 1, conservation of charge at the jth node yields

$$i_{B,j} + \sum_{\langle k \rangle} \left[i_{c,jk} \sin(\theta_j - \theta_k) + \frac{d}{d\tau}(\theta_j - \theta_k) + \beta_c \frac{d^2}{d\tau^2}(\theta_j - \theta_k) \right] = 0. \quad (1)$$

Here θ_j is the Josephson phase at *node* j, and $i_{c,jk} \equiv I_{c,jk}/I_{cx}$ is the dimensionless critical current of the junction between nodes j and k. The sum runs over all nearest-neighbor nodes to j. We allow for critical current anisotropy in that I_{cx} and I_{cy} need not be equal. In fact we will define a measure of the critical current anisotropy as $\alpha \equiv I_{cy}/I_{cx}$. The McCumber parameter β_c was defined in Sec. I. The array is not subjected to any *external* magnetic field. Equation (1) is combined with the standard Josephson voltage expression for node j, $V_j = (\hbar/2e)(d\theta_j/dt)$, which if we define a characteristic voltage $V_c \equiv I_{cx}R$, can be written in dimensionless form

$$v_j \equiv \frac{V_j}{V_c} = \frac{d\theta_j}{d\tau}. \quad (2)$$

We have solved Eqs. (1) and (2) numerically using the fourth-order Runge-Kutta method, with (dimensionless) time steps of $\Delta\tau = 0.001$. Typically, the code was run for at least a time of $\tau_{total} = 500\,000$ to allow the horizontal junctions to phase lock. Then the Floquet (stability) analysis was performed, which we now describe.

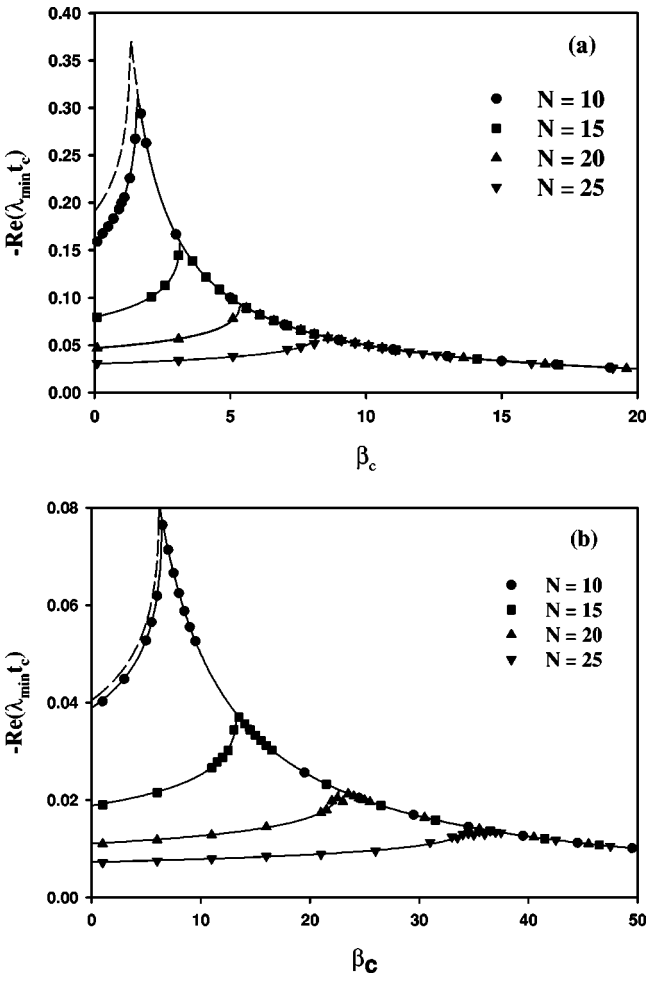

FIG. 2. Magnitude of the minimum Floquet exponent vs the dimensionless junction capacitance for four different ladder sizes. The bias current was fixed at $i_B = 10$, and the critical-current anisotropy factor was $\alpha = 1$. The solid lines are the result of an analytic calculation [Eq. (14)] based on the full RCSJ equations. The dashed lines demonstrate, for $N = 10$, the analytic result based on a DSG equation for the horizontal junctions. (a) Periodic boundary conditions. (b) Open boundary conditions.

Suppose that $\theta_{0j}(\tau)$ is a solution to Eqs. (1) and (2). We perturb the phase at node j by an amount $\eta_j(\tau)$ so that the new phase is $\theta_j(\tau) = \theta_{0j}(\tau) + \eta_j(\tau)$. Linearizing Eq. (1) with respect to η_j, we arrive at the following:

$$\sum_{\langle k \rangle} \left[i_{c,jk} \cos(\theta_{0j} - \theta_{0k})(\eta_j - \eta_k) + \frac{d}{d\tau}(\eta_j - \eta_k) + \beta_c \frac{d^2}{d\tau^2}(\eta_j - \eta_k) \right] = 0. \quad (3)$$

Because the coefficients of the η_j are periodic in time, with period T/t_c in dimensionless units, we can apply Floquet's theorem [34], which tells us that there exist solutions to Eq. 3 of the form

$$\eta_j\left(\tau+\frac{T}{t_c}\right)=\mu\,\eta_j(\tau), \tag{4}$$

where μ is a (possibly complex) number called the Floquet multiplier. We are interested in the case when $|\mu|<1$, which corresponds to perturbations that diminish with time. Of course, $|\mu|>1$ denotes instability in that perturbations grow over time, and the special case of $|\mu|=1$ is called neutral stability. There is a corresponding Floquet exponent λ, which is related to the Floquet multiplier by

$$\mu=e^{\lambda T}=e^{(\lambda t_c)(T/t_c)}. \tag{5}$$

The condition $|\mu|<1$ corresponds to $\mathrm{Re}(\lambda)<0$. We can think physically of the exponents (or multipliers) as describing the stability of the characteristic modes of the array. *At least* one of these exponents must equal zero, which is a result of the invariance of Eq. (1) to a time translation. Excluding the exponent of zero, we are interested in the remaining exponent of *smallest magnitude*, $|\lambda_{\min}|$, as that tells us by what factor the longest-lived mode of the array decays (or grows) in one period after a perturbation [35].

We have performed a linear stability analysis for ladders of size $N=10$, 15, 20, and 25 with $1\leqslant\beta_c\lesssim 50$ and $i_B=10$. Consider Fig. 2(a) that shows $-\mathrm{Re}(\lambda_{\min}t_c)$ vs β_c for $\alpha=1$ in a ladder with *periodic* boundary conditions. The behavior observed here has been previously reported [21], so we will only summarize the key results. There is a general trend for decreasing β_c of increasing stability (as demonstrated by a growing magnitude of the Floquet exponent) down to a crossover value of the McCumber parameter $\beta_c^*(N)$, which is dependent upon ladder size. For decreasing β_c below $\beta_c^*(N)$, the phase locking takes increasingly longer to recover from a mechanical perturbation. As is seen from the figure, this crossover behavior of the stability is a sharp function of β_c. Furthermore, above the crossover $[\beta_c>\beta_c^*(N)]$, the Floquet exponent has a simple form, namely, $\mathrm{Re}(\lambda_{\min}t_c)=-1/2\beta_c$, which holds for all ladder sizes and bias currents we have looked at (as long as the ladder is in the whirling regime, of course). For reasons discussed previously [21], we find it convenient to describe the ladder's behavior as overdamped for $\beta_c<\beta_c^*(N)$ and underdamped for $\beta_c>\beta_c^*(N)$. Physically, the sharp change in stability at $\beta_c^*(N)$ is due to one of the small-amplitude, oscillatory modes of the ladder becoming less efficient at damping out perturbations.

Figure 2(b) shows the minimum Floquet exponents for a ladder with *open* boundary conditions. A comparison of Figs. 2(a) and 2(b) shows two important differences. The position of the crossover value $\beta_c^*(N)$ for a given ladder size is increased in the open ladder relative to the periodic ladder [note the different horizontal scales in Figs. 2(a) and 2(b)], i.e., less damping per junction is needed, for a given ladder size, in the open ladder before the crossover to overdamped behavior results. Also, in the overdamped regime, $|\mathrm{Re}(\lambda_{\min}t_c)|$ is smaller by approximately a factor of 0.25 in the open ladder than in its periodic counterpart. That is, the phase-locked solutions for the open ladder in the overdamped regime are *less stable* than for the periodic ladder.

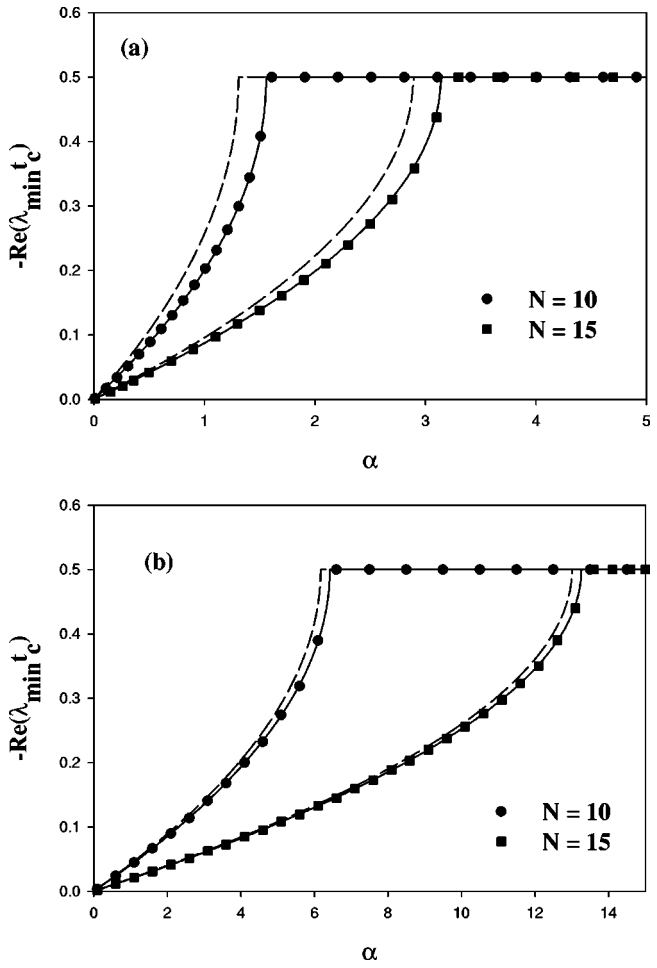

FIG. 3. Minimum Floquet exponent for overdamped ladders ($\beta_c=1$) vs the critical-current anisotropy for two different ladder sizes. The exponent equals $-1/2\beta_c$ independent of N and α for α greater than some crossover value, $\alpha^*(N)$, which is dependent on ladder size. The solid lines are the result of an analytic calculation [Eq. (14)] based on the full RCSJ equations. The dashed line demonstrates, for $N=10$, the analytic result based on a DSG equation for the horizontal junctions. (a) Periodic boundary conditions. (b) Open boundary conditions.

Figures 3(a) and 3(b) compare the exponents for both periodic and open ladders as a function of the critical current anisotropy α for $N=10$ and 15 and for $\beta_c=1.0$. In this case, as α is decreased, there is a crossover value $\alpha^*(N)$ that is a function of ladder size. For $\alpha>\alpha^*(N)$ the minimum exponent is constant at $-1/2\beta_c$, while for $\alpha<\alpha^*(N)$ the exponent decreases towards zero as α approaches zero. A Floquet exponent of zero (or a Floquet *multiplier* of unity) denotes neutral stability. We would expect the array to exhibit a high degree of neutral stability in the limit in which the horizontal junctions were decoupled. This is just what $\alpha\rightarrow 0$ represents. So the behavior of the exponents for $I_{cy}\ll I_{cx}$ is as expected. As was the case in Figs. 2(a) and 2(b), we see that for $\alpha<\alpha^*(N)$ the open ladder is less stable than the periodic ladder. Further insight into the behavior exhibited in both Figs. 2 and 3 is gained by considering the analytic calculation of the exponents, which we now discuss.

B. Analytic results

We find it convenient at this point to introduce a change in notation. Let ϕ_j represent the Josephson phase for the jth horizontal junction. For example, based on Fig. 1, $\phi_1=\theta_1-\theta_2$. Also, let $\psi_{1j}(\psi_{2j})$ be the Josephson phase for a vertical junction corresponding to $x=0(x=a)$, i.e., $\psi_{11}=\theta_1-\theta_3$ and $\psi_{21}=\theta_2-\theta_4$. We shall take advantage of the well-known symmetry of the array that results in $\psi_{1j}=-\psi_{2j}$, as can be verified from the RCSJ equations [36], to simplify the analysis. Applying conservation of charge to the left node of the jth horizontal junction results in

$$i_B-\alpha\sin\psi_{j-1}-\frac{d\psi_{j-1}}{d\tau}-\beta_c\frac{d^2\psi_{j-1}}{d\tau^2}-\sin\phi_j-\frac{d\phi_j}{d\tau}$$

$$-\beta_c\frac{d^2\phi_j}{d\tau^2}+\alpha\sin\psi_j+\frac{d\psi_j}{d\tau}+\beta_c\frac{d^2\psi_j}{d\tau^2}=0. \tag{6}$$

In addition, we include the constraint that in the absence of any external or induced magnetic flux through a given plaquette, the sum of the gauge-invariant phase differences around a plaquette must vanish [37]. In our case, for the plaquette consisting of the horizontal junctions j and $j+1$ and the corresponding vertical junctions we have

$$\phi_j-\phi_{j+1}+2\psi_j=0, \tag{7}$$

where we have made the definition $\psi_{1j}=-\psi_{2j}\equiv\psi_j$. We then solve Eq. (7) for ψ_j and substitute into Eq. (6). Similarly, we can write the phase constraint for the plaquette consisting of horizontal junctions j and $j-1$, solve for ψ_{j-1}, and substitute into Eq. (6). The result is an equation depending on phase differences for only the horizontal junctions,

$$\frac{\beta_c}{2}\nabla^2\left(\frac{d^2\phi_j}{d\tau^2}\right)+\frac{1}{2}\nabla^2\left(\frac{d\phi_j}{d\tau}\right)-\beta_c\frac{d^2\phi_j}{d\tau^2}-\frac{d\phi_j}{d\tau}-\sin\phi_j$$

$$+\alpha\left[\sin\left(\frac{\phi_{j+1}-\phi_j}{2}\right)+\sin\left(\frac{\phi_{j-1}-\phi_j}{2}\right)\right]+i_B=0, \tag{8}$$

where we have introduced the discrete Laplacian notation $\nabla^2 f_j\equiv f_{j+1}-2f_j+f_{j-1}$ for a function f_j defined on the array.

Note that a DSG equation results from Eq. (8) by ignoring the Laplacians of the time derivatives and also by linearizing the sine terms in the square brackets. Such a simplification is based on the assumption that the Josephson phase differences for the horizontal junctions are only weak functions of position as one moves along the ladder. Such simplifications result in

$$\beta_c\frac{d^2\phi_j}{d\tau^2}+\frac{d\phi_j}{d\tau}+\sin\phi_j-\frac{\alpha}{2}\nabla^2\phi_j-i_B=0. \tag{9}$$

It is worthwhile to understand better under what conditions Eqs. (8) and (9) are indeed dynamically equivalent. One probe of such conditions is the set of Floquet exponents that result from these equations. A previous calculation of the exponents for Eq. (9) based on periodic boundary conditions has been discussed elsewhere [21]. We shall merely quote the result,

$$\mathrm{Re}(\lambda_m^{(DSG)}t_c)=-\frac{1}{2\beta_c}\pm\frac{1}{2\beta_c}\mathrm{Re}\sqrt{1-4\beta_c[\omega_m^{(DSG)}]^2}, \tag{10}$$

where $[\omega_m^{(DSG)}]^2=2\alpha\sin^2(m\pi/N)(m=0,1,\ldots,N-1)$ is a set of characteristic, or normal-mode, frequencies for a *parallel* array of N junctions. That is, $\omega_m^{(DSG)}$ describe the frequencies of the small-amplitude phase oscillations of the underdamped ladder array in which the *vertical* junctions have been shorted. The agreement of Eq. (10) with the numerical exponents for the *full* RCSJ ladder is good in the underdamped regime $[\beta_c>\beta_c^*(N)]$, but there is a quantitative difference in the overdamped regime, as observed in Fig. 2(a) for $N=10$. [The dashed line represents the prediction of Eq. (10).] Some physics, that becomes increasingly important in the overdamped limit, was discarded in simplifying Eq. (8) to get to Eq. (9). That physics is the spatial variation of the ϕ_j, and their time derivatives, along the ladder.

We have calculated the Floquet exponents analytically for Eq. (8) directly. As described in Sec. II and in Ref. [21], we let $\phi_j=\phi_{0j}+\eta_j$ and linearize with respect to the η_j. We also assume that the unperturbed phases are growing linearly with time at a common rate, i.e., $\phi_{0j}=\omega\tau$, as is characteristic of the whirling regime. The resulting equation, linear in the η_j, is

$$\frac{\beta_c}{2}\nabla^2\left(\frac{d^2\eta_j}{d\tau^2}\right)+\frac{1}{2}\nabla^2\left(\frac{d\eta_j}{d\tau}\right)-\beta_c\frac{d^2\eta_j}{d\tau^2}-\frac{d\eta_j}{d\tau}-\cos(\omega\tau)\,\eta_j$$

$$-\frac{\alpha}{2}\nabla^2\eta_j=0. \tag{11}$$

Based on the assumption of periodic boundary conditions, we expand the η_j in an appropriate Fourier series

$$\eta_j=\sum_{m=0}^{N-1}A_m(\tau)e^{2\pi imj/N} \tag{12}$$

and substitute back into Eq. (11). After some algebra and using the fact that the Fourier modes are independent of each other we arrive at a differential equation for the Fourier coefficients

$$\left[1+2\sin^2\left(\frac{m\pi}{N}\right)\right]\left\{\frac{d^2A_m}{d\tau^2}+\frac{1}{\beta_c}\frac{dA_m}{d\tau}\right\}$$

$$+\frac{1}{\beta_c}\left[2\alpha\sin^2\left(\frac{m\pi}{N}\right)+\cos(\omega\tau)\right]A_m=0. \tag{13}$$

This is a Mathieu's equation with damping and is almost identical in form to that studied in Ref. [21] for the periodic DSG equation. A key difference with this new result, however, is the presence of the m-dependent sine terms multiplying the time derivatives of the A_m. It turns out that these

terms play an important role in determining the Floquet exponents for small β_c. An analysis of Eq. (13) similar to that described in Ref. [21] yields the result

$$\mathrm{Re}(\lambda_m^{(RCSJ)} t_c) = -\frac{1}{2\beta_c} \pm \frac{1}{2\beta_c}\mathrm{Re}\sqrt{1-4\beta_c[\omega_m^{(RCSJ)}]^2}, \tag{14}$$

where now the characteristic frequencies are given by

$$[\omega_m^{(RCSJ)}]^2 = \frac{2\alpha \sin^2\left(\frac{m\pi}{N}\right)}{1+2\sin^2\left(\frac{m\pi}{N}\right)}. \tag{15}$$

We see that the inclusion of the Laplacians $\nabla^2(d^2\eta_j/d\tau^2)$ and $\nabla^2(d\eta_j/d\tau)$ in Eq. (11) has resulted in a new, effective set of normal-mode frequencies. In effect, the spatial variation of the time derivatives has renormalized the frequencies for a *parallel* array by a factor of $[1+2\sin^2(m\pi/N)]^{-1}$. It is Eq. (14) that we now compare with the numerical results for the exponents, as shown in Figs. 2 and 3 [38].

Consider the set of all possible exponents resulting from Eq. (14) when the normal mode index runs over its range, $0 \leqslant m \leqslant N-1$. For the $m=0$ mode, we see that the two possible values are $\mathrm{Re}(\lambda_0 t_c)=0, -1/\beta_c$, where, in fact, $-1/\beta_c$ is the largest possible magnitude exponent one can obtain from Eq. (14) and represents the fastest decaying mode of the array. For all modes $m>0$, the possible exponents can be divided into two categories, depending on whether the argument of the square root in Eq. (14) is less than or greater than zero. We shall refer to the case of when the argument of the square root is less (greater) than zero as the ''overdamped'' (''underdamped'') regime. Thus we have

$$\mathrm{Re}(\lambda_m^{(RCSJ)} t_c) = \begin{cases} -\dfrac{1}{2\beta_c} & \text{if } 4\beta_c[\omega_m^{(RCSJ)}]^2 > 1 \\ -\dfrac{1}{2\beta_c}\left[1 \pm \sqrt{1-4\beta_c[\omega_m^{(RCSJ)}]^2}\right] & \text{if } 4\beta_c[\omega_m^{(RCSJ)}]^2 < 1. \end{cases} \tag{16}$$

Figures 2(a) and 3(a) offer a comparison of the numerical and analytic results for the Floquet exponents for several periodic ladder sizes and zero external field. The analytic results, shown as line plots, were obtained by plotting, for a given β_c, α, and N, the exponent from Eq. (16) with the *smallest magnitude*. We see that the agreement is excellent. For further comparison we also show (for $N=10$) the analytic result, Eq. (10), based on the DSG equation. It is clear that the DSG result overestimates the exponents in the overdamped regime. This difference is due to neglect (in the DSG equation) of the Laplacian terms of the time derivatives as mentioned in the previous paragraph. Clearly, the spatial variation represented by these terms and the appropriate spectrum for small amplitude phase oscillations ($\omega_m^{(RCSJ)}$ vs $\omega_m^{(DSG)}$) are important in understanding the dynamics in the overdamped regime.

A similar analytic analysis can be performed for the open ladder. The key difference is the form of the Fourier series used to represent the perturbations [31]:

$$\eta_j = \sum_{m=0}^{N-1\prime} A_m(\tau)\cos\left[\frac{m\pi\left(j-\frac{1}{2}\right)}{N+1}\right], \tag{17}$$

where the prime on the summation means there is a factor of one-half in front of the sum for the $m=0$ mode only. The same method applied to the periodic ladder leads to an equation of the same form as Eq. (14) but with the following characteristic frequencies

$$[\omega_m^{(RCSJ,open)}]^2 = \frac{2\alpha \sin^2\left(\frac{m\pi}{2[N+1]}\right)}{1+2\sin^2\left(\frac{m\pi}{2[N+1]}\right)}. \tag{18}$$

These frequencies result in the solid lines of Figs. 2(b) and 3(b). As in the case of the periodic ladder, the agreement between this new analytic result and the numerical results is excellent.

Further observation of Fig. 2(b) shows that (for $N=10$) the analytic result based on the DSG equation, with $[\omega_m^{(DSG)}]^2 = 2\alpha\sin^2(m\pi/2[N+1])$, and the analytic result based on Eq. (18) do not differ significantly. This is in contrast to the periodic ladder of the same size. In effect, the difference in boundary conditions has led to different renormalization factors for the characteristic frequencies, with different sine terms in the denominators. [Compare Eqs. (15) and (18).] In the open ladder, the extra factor of 2 that appears in the denominator of the argument of the sine suppresses its importance for all but the smallest ladders. In fact, a quantitative way to gauge the importance of the renormalization of the characteristic frequencies and in turn the importance of the Laplacian terms in Eq. (11) is to calculate the relative difference between the minimum exponents based on Eqs. (14) and (10) (both analytic results) for several different values of N and β_c and for both periodic and open ladders. That is, we plot $|\mathrm{Re}(\lambda_{\min}^{(RCSJ)} t_c) - \mathrm{Re}(\lambda_{\min}^{(DSG)} t_c)|/|\mathrm{Re}(\lambda_{\min}^{(RCSJ)} t_c)|$ vs β_c for $N=10$, 15, 20, and 25 (see Fig. 4). We see that the two sets of analytic results for periodic ladders can differ by as much 50% in the overdamped regime. For open ladders,

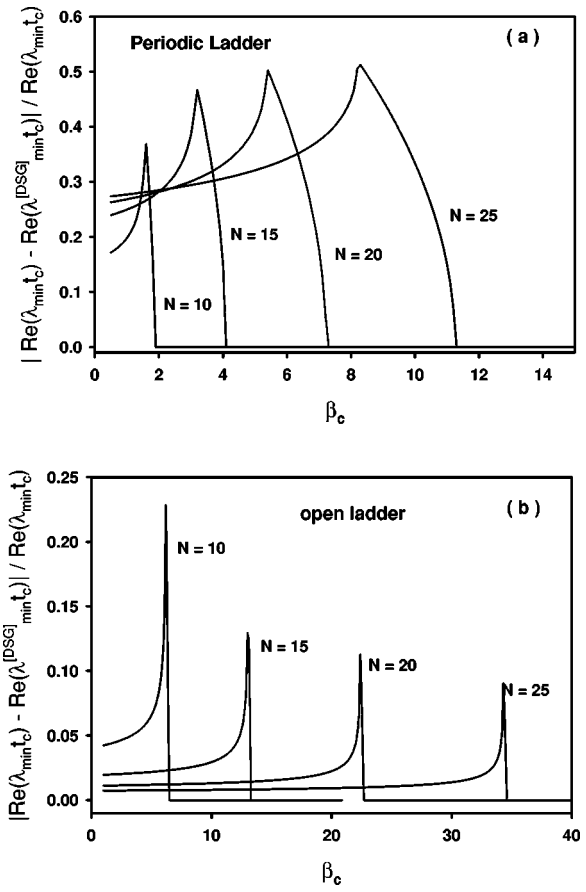

FIG. 4. Relative difference between the two analytic results [Eqs. (10) and (14)] for the minimum Floquet exponent as a function of the dimensionless capacitance of the junctions. (The results correspond to $\alpha=1$.) $\mathrm{Re}(\lambda_{\min}t_c)$ represents the result [Eq. (14)] based on the full RCSJ equations, while $\mathrm{Re}(\lambda_{\min}^{[DSG]}t_c)$ represents the result [Eq. (10)] based on a DSG equation for the horizontal junctions. (a) Periodic boundary conditions. (b) Open boundary conditions.

the maximum relative difference is at most roughly half that of their periodic counterparts. Furthermore, for a given value of N, the open ladders yield a sharp peak in the relative difference as a function of β_c, whereas the periodic ladders experience a broader range of β_c values over which the difference is sizeable. The upshot is that the geometry, i.e., boundary conditions, of the array has a significant effect upon the stability of phase-locked solutions in the overdamped regime. In addition, an analysis of the ladder based on the DSG equation will overestimate the Floquet exponents at small β_c. This is because the DSG equation neglects spatial variations of the derivatives $d\phi_j/d\tau$ and $d^2\phi_j/d\tau^2$ along the ladder.

III. SELF-INDUCTANCE

A. Numerical results

Several groups over the last decade have discussed the importance of including current-induced magnetic fields in a study of the static and dynamic properties of Josephson junction arrays [36,39–45]. It is natural then to ask about the effects of such induced magnetic fields on the stability of phase-locked solutions. We address this issue in Secs. III–V of the paper. We start by considering each plaquette in a *periodic* ladder to be described by some self-inductance L. We also adopt a mesh current approach [46], in which we assume that the jth plaquette is described by a well-defined circulating mesh current I_j (see Fig. 5). Applying conservation of charge to the upper left node of the jth plaquette gives, in dimensionless units,

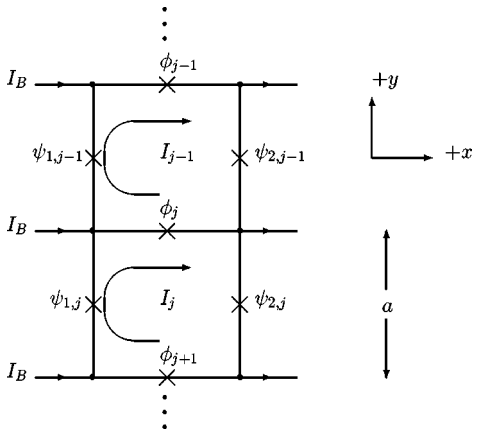

FIG. 5. Two plaquettes in a ladder array with N plaquettes ($N>2$). ϕ_j represents the Josephson phase for the jth horizontal junction, which also comprises the top junction in the jth plaquette. ψ_{1j} (ψ_{2j}) represents the Josephson phase for the vertical junction on the left (right) side of the jth plaquette. I_j is the mesh current circulating in the jth plaquette.

$$i_B+i_j-i_{j-1}=\sin\phi_j+\frac{d\phi_j}{d\tau}+\beta_c\frac{d^2\phi_j}{d\tau^2}, \tag{19}$$

where $i_j\equiv I_j/I_{cx}$ is the dimensionless mesh current in plaquette j. Similarly, the vertical junction on the left side of plaquette j is described by

$$i_j=\alpha\sin\psi_j+\frac{d\psi_j}{d\tau}+\beta_c\frac{d^2\psi_j}{d\tau^2}, \tag{20}$$

where as before $\alpha\equiv I_{cy}/I_{cx}$ measures the critical-current anisotropy in the ladder. Finally, the constraint on the Josephson phases yields (for plaquette j) [37]

$$\phi_j-\phi_{j+1}+2\psi_j=-\frac{2\pi}{\Phi_0}\Phi_j, \tag{21}$$

where $\Phi_0\equiv h/2e$ is the magnetic flux quantum, and Φ_j is the total magnetic flux passing through plaquette j. In the absence of any external flux, and considering only the self-inductance of a given plaquette means that $\Phi_j=LI_j$. So Eq. (21) can be written as

$$\phi_j - \phi_{j+1} + 2\psi_j = -\frac{2\pi L I_{cx}}{\Phi_0} i_j ,$$

and introducing a dimensionless loop inductance $\beta_L \equiv 2\pi L I_{cx}/\Phi_0$ gives us the following useful form of the phase constraint equation:

$$\phi_j - \phi_{j+1} + 2\psi_j = -\beta_L i_j . \tag{22}$$

The next step is to solve Eq. (22) for i_j and substitute into Eq. (19). Also, by making the change of notation $j \to j-1$ in Eq. (22) we obtain a constraint equation for i_{j-1} in terms of phase differences that can also be substituted into Eq. (19). The resultant equation is independent of the mesh currents and takes the form

$$\beta_c \frac{d^2\phi_j}{d\tau^2} + \frac{d\phi_j}{d\tau} + \sin\phi_j - \frac{1}{\beta_L}(\nabla^2\phi_j - 2[\psi_j - \psi_{j-1}]) - i_B = 0. \tag{23}$$

Eliminating the mesh current i_j from Eq. (20) yields

$$\beta_c \frac{d^2\psi_j}{d\tau^2} + \frac{d\psi_j}{d\tau} + \alpha \sin\psi_j + \frac{1}{\beta_L}(\phi_j - \phi_{j+1} + 2\psi_j) = 0. \tag{24}$$

Equations (23) and (24) were solved numerically for ϕ_j, ψ_j, $d\phi_j/d\tau$, and $d\psi_j/d\tau$. Next, to find the Floquet exponents we perform a linear stability analysis. Let $\phi_j = \phi_{0j} + \eta_j$ and $\psi_j = \psi_{0j} + \delta_j$, where ϕ_{0j} and ψ_{0j} are solutions to Eqs. (23) and (24). Substituting these perturbed phases into Eqs. (23) and (24) and linearizing with respect to η_j and δ_j gives

$$\beta_c \frac{d^2\eta_j}{d\tau^2} + \frac{d\eta_j}{d\tau} + (\cos\phi_{0j})\eta_j - \frac{1}{\beta_L}(\nabla^2\eta_j - 2[\delta_j - \delta_{j-1}]) = 0 \tag{25}$$

and

$$\beta_c \frac{d^2\delta_j}{d\tau^2} + \frac{d\delta_j}{d\tau} + \alpha(\cos\psi_{0j})\delta_j + \frac{1}{\beta_L}(\eta_j - \eta_{j+1} + 2\delta_j) = 0. \tag{26}$$

The resulting minimum Floquet exponents, calculated numerically based on Eqs. (23)–(26) as a function of the dimensionless loop inductance β_L, are shown in Fig. 6 for periodic ladders. Figure 6(a) corresponds to a ten-cell ladder with $\beta_c = 10$ and three different values of the critical-current anisotropy, α. (All the numerical values of the exponents shown in Fig. 6 were calculated by initializing the phases to zero and the voltages randomly.) We would roughly categorize the results as belonging to one of three different regimes: in the capacitive regime (valid for $\beta_c \gtrsim \beta_L$) we find the minimum Floquet exponent equal to $-1/2\beta_c$ independent of β_L; in the inductive regime (valid for $\beta_L \gg \beta_c$) we find the exponent is proportional to $-1/\beta_L$, independent of β_c; and then for $\beta_L \approx \beta_c$ both the junction capacitance and loop inductance affect the size of the exponent. Also note that the exponents exhibit a dependence on the value of α for $15 \lesssim \beta_L \lesssim 30$ and $\beta_c = 10$. Specifically, for β_L values in this range, as α is decreased the degree of stability is reduced, as is evidenced by a smaller exponent. Figure 6(b) shows similar behavior for $\beta_c = 30$. Figure 7 shows the results of the same calculations for open ladders as opposed to periodic ladders. A comparison of Figs. 6 and 7 in the inductive regime shows that the exponents are larger in magnitude for the periodic ladder, demonstrating (as in Sec. II) that, generally speaking, the periodic ladder is more stable than the open ladder. It is worth noting that for $\beta_c = 10$ and $\beta_c = 30$ both types of ladders, periodic and open, show $-1/2\beta_c$ behavior in the capacitive regime. Although we have not checked explicitly, we would expect that for small enough capacitance ($\beta_c \lesssim 2$), the periodic and open ladders would have differing exponents even in the capacitance regime, with the periodic ladder more stable.

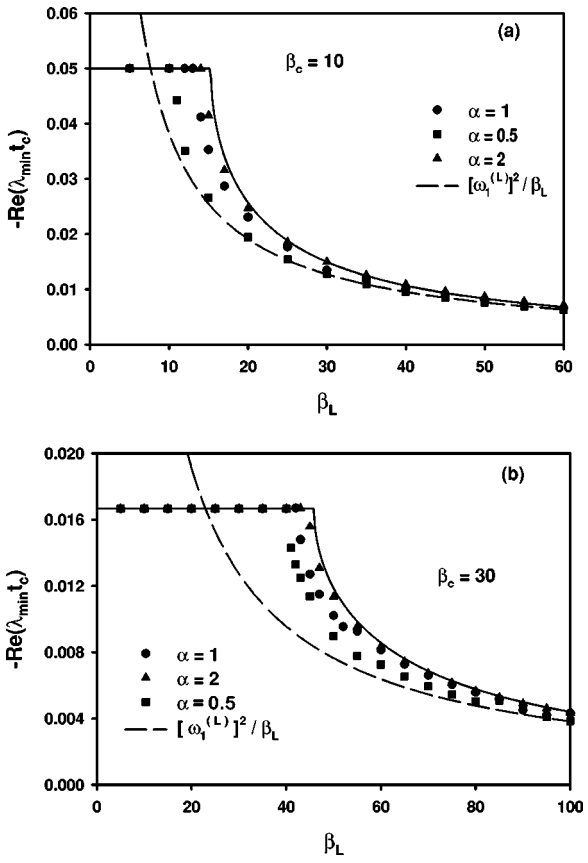

FIG. 6. Minimum Floquet exponent vs dimensionless self-inductance of a plaquette for $i_B = 10$ and three different values of the critical-current anisotropy in a ladder with $N = 10$ and *periodic* boundary conditions. The solid line represents an analytic result [Eq. (28)] based on a DSG equation for the horizontal junctions. The dashed line is the large β_L limit of the analytic result, where $\omega_1^{(L)}$ is one of the normal-mode frequencies of a parallel array of junctions. (a) $\beta_c = 10$. (b) $\beta_c = 30$.

To help the reader visualize the dependence of the Floquet exponent on both the junction capacitance and the loop inductance, consider Fig. 8, which represents the minimum

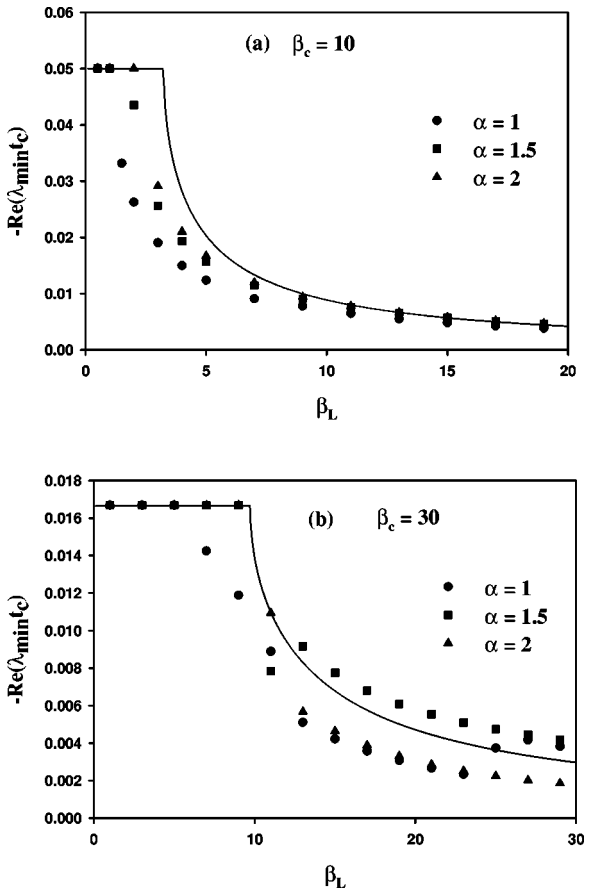

FIG. 7. Minimum Floquet exponent vs dimensionless self-inductance of a plaquette for $i_B=10$ and three different values of the critical-current anisotropy in a ladder with $N=10$ and *open* boundary conditions. The solid line represents an analytic result [Eq. (28)] based on a DSG equation for the horizontal junctions. (a) $\beta_c=10$. (b) $\beta_c=30$.

exponent as a function of both β_c and β_L for a periodic ladder with $N=5$. This plot was produced by calculating the exponents for hundreds of different combinations of the two parameters. Our plotting program then interpolated between the data points to produce the surface shown in the figure. Inspection reveals that the behavior represented in Figs. 6 and 7 is obtained by merely taking an appropriate cross-sectional slice through Fig. 8.

B. Analytical results

First-order versions of Eqs. (23) and (24) in the overdamped limit ($\beta_c \to 0$) have been studied by Filatrella and Wiesenfeld [36] via an iterative approach. We employ a similar method here. To make analytic progress towards understanding the behavior of Figs. 6 and 7, we start by neglecting the phase differences associated with the *vertical* junctions in Eq. (23). As partial justification for this step, we check numerically that over a wide range of values of N, β_c, and β_L, and for random initial values of all the phases, the vertical phase differences, ψ_j, do indeed approach zero. In this limit, Eq. (23) reduces to a DSG equation for the ϕ_j,

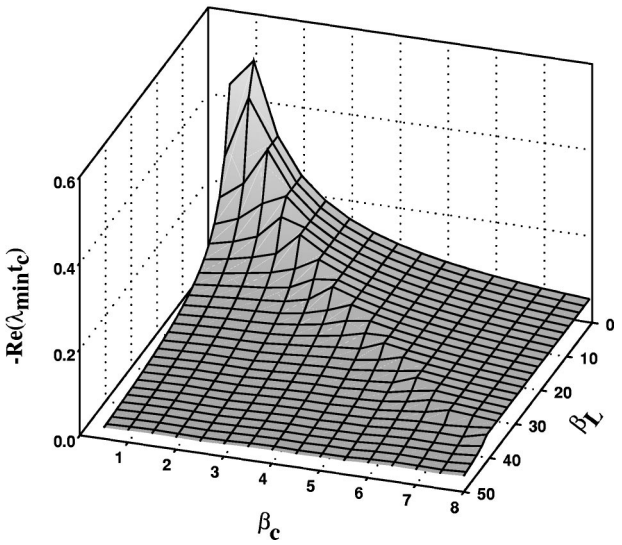

FIG. 8. Minimum Floquet exponent vs dimensionless junction capacitance and dimensionless loop self-inductance for $i_B=10$ and $N=5$ in a ladder with periodic boundary conditions. The crossover ridge demarking the border between the capacitive and inductive regimes is visible roughly through the middle of the β_c-β_L plane. This plot was produced by numerically evaluating the minimum exponent for hundreds of combinations of β_c and β_L values.

$$\beta_c \frac{d^2\phi_j}{d\tau^2} + \frac{d\phi_j}{d\tau} + \sin\phi_j - \frac{1}{\beta_L}\nabla^2\phi_j - i_B = 0. \qquad (27)$$

Note that in contrast to Sec. II, where the critical-current anisotropy controlled the coupling strength of nearest-neighbor horizontal junctions, in this case of a self-inductive ladder the inverse of the loop inductance determines the coupling strength. Also, it is important to remember that Eq. (27) is only an adequate reflection of the of the dynamics of the ladder in the case when $\psi_j \to 0$, i.e., the vertical junctions are inactive.

Because Eq. (27) has the form of a DSG equation for the phases ϕ_j we can calculate analytically a corresponding set of Floquet exponents in a manner identical to that described in Sec. II. The result is

$$\mathrm{Re}(\lambda_m^{(L)} t_c) = -\frac{1}{2\beta_c} \pm \frac{1}{2\beta_c}\mathrm{Re}\sqrt{1 - 4[\omega_m^{(L)}]^2\left(\frac{\beta_c}{\beta_L}\right)}, \qquad (28)$$

where the characteristic frequencies are $[\omega_m^{(L)}]^2 = 4\sin^2(m\pi/N)$ $(m=0,1,\ldots,N-1)$ for a *periodic* ladder. Equation (28) yields the solid lines in Figs. 6 and 7. For the open ladder the frequencies are $[\omega_m^{(L,open)}]^2 = 4\sin^2(m\pi/2[N+1])$. With the aid of Eq. (28) we can identify more precisely the capacitive and inductive regimes for the ladder. In the capacitive regime, $4[\omega_m^{(L)}]^2\beta_c/\beta_L > 1$ or $\beta_c > \beta_L/4[\omega_m^{(L)}]^2$ such that $\mathrm{Re}(\lambda_m^{(L)} t_c) = -1/2\beta_c$, independent of β_L. In the inductive regime, $4[\omega_m^{(L)}]^2\beta_c/\beta_L \ll 1$ or $\beta_L \gg 4[\omega_m^{(L)}]^2\beta_c$ such that the *minimum* Floquet exponent follows from Eq. (28)

$$\mathrm{Re}(\lambda_{\min}^{(L)} t_c) \approx -\frac{[\omega_1^{(L)}]^2}{\beta_L}, \tag{29}$$

independent of β_c. Note that Fig. 6 includes a graph of this limiting result [Eq. (29)] for the inductive regime (see the dashed line).

A comparison of the numerical and analytical results in Figs. 6 and 7 show good agreement in the capacitive and inductive regimes, but for $\beta_c \approx \beta_L$ there is a noticeable discrepancy. It is important to note that our analytic result is independent of the critical-current anisotropy α since that affects the ϕ_j only through coupling with the ψ_j. Presumably, then, the difference between the analytical and numerical results is due to our neglecting the vertical junctions entirely. Thus we turn to Eq. (26).

We now assume that the perturbations to the vertical phase differences δ_j can be expanded in a Fourier series

$$\delta_j = \sum_{m=0}^{N-1} B_m(\tau) e^{2\pi i m j/N}, \tag{30}$$

and we also use our previous Fourier series for the η_j (see Sec. II) to write Eq. (26) as a differential equation for the coefficients B_m and the A_m. At this point, we also take into account that when running our code that calculates the exponents numerically we always initialized the phases to zero. That means that we expect $\psi_{0j} = \psi_0$, independent of j. (Recall, that as part of the numerical process for calculating the exponents, we integrate Eqs. (23) and (24) for at least 500 000 time steps before applying the perturbation. ψ_{0j} represents the phase difference across the jth vertical junction *just before the perturbation*. Numerical evidence suggests that if the phases are initialized uniformly, they remain uniform along the ladder (modulo 2π). Also, recall that the *voltages* across all the junctions throughout the array are initialized randomly.) The resulting equation describing the Fourier modes of the vertical junctions is

$$\beta_c \frac{d^2 B_m}{d\tau^2} + \frac{dB_m}{d\tau} + \left(\alpha \cos\psi_0 + \frac{2}{\beta_L}\right) B_m = \frac{1}{\beta_L}(e^{2\pi i m/N} - 1) A_m. \tag{31}$$

Now according to Floquet theory [34], the $A_m(\tau)$, which describe the perturbed horizontal junctions, can be written in the form

$$A_m(\tau) = e^{\lambda_m^{(L)} t_c \tau} \rho_m(\tau), \tag{32}$$

where in our case $\rho_m(\tau)$ is an unknown, periodic function of time. That is, although we have been able to solve for the Floquet exponents, $\lambda_m^{(L)}$ [Eq. (28)], we do not know the form of the ρ_m, and so the right side of Eq. (31) is not a completely known function of time. With the hope of learning *something* about the behavior of the vertical junctions we can solve the homogeneous version of Eq. (31). That is, we set the right side to zero and assume a solution of the form $B_m(\tau) = e^{\Lambda t_c \tau}$. The resulting quadratic equation for the exponents Λ can be solved to give

$$\Lambda^{(\pm)} t_c = -\frac{1}{2\beta_c} \pm \frac{1}{2\beta_c}\sqrt{1 - 4\beta_c\left(\alpha \cos\psi_0 + \frac{2}{\beta_L}\right)}. \tag{33}$$

Note that the solutions for the B_m will exponentially grow with time and hence represent an instability in the ladder, if $\Lambda^{(+)} t_c > 0$. This can occur if

$$\alpha < -\frac{2}{\beta_L \cos\psi_0}, \tag{34}$$

where we remind the reader that ψ_0 is the phase difference across a vertical junction just prior to the perturbation. Once again, numerical evidence suggests that if the phases are initialized to zero, then $\psi_0 \approx 0 \bmod(2\pi)$. Thus we can say $\cos\psi_0 \approx 1$ in Eq. (34). It is clear that the inequality can never be satisfied since β_L and α are non-negative quantities, and the solution to the homogeneous part of Eq. (31) describes exponentially *decaying* functions of time.

It remains to find a particular solution to Eq. (31). Unfortunately, this is not possible since the full functional form of the A_m is unknown. We can guess, however, that any particular solution will have the same general form as that of the A_m, namely, a decaying exponential function of time multiplying a periodic function of time [see Eq. (32)]. The full solution to Eq. (31) is thus a sum of the homogeneous and particular solutions, i.e., a sum of exponentially decaying solutions where the set of all possible ''decay rates'' is given by Eqs. (28) and (33). The upshot is that an analytic result for the Floquet exponents for the full *coupled* Eqs. (25) and (26) has yet to be attained. Such a solution is required to explain the α dependence of the numerical results seen in Figs. 6 and 7.

One useful check of our analytic work on the vertical junctions is to see if the analytic exponents obtained for the homogeneous version of Eq. (31) describe *any* of the set of $4N$ (for periodic ladders) exponents calculated numerically directly from Eqs. (25) and (26). For example, Table I gives the exponents for a five-cell periodic ladder with $\beta_c = 1$, $\beta_L = 50$, and $\alpha = 0.1$, corresponding to a region where the numerical and analytical results for $\lambda_{\min}$ differ. We can easily identify the exponents with approximate values of zero and $-1/\beta_c$. These would be expected based on Eq. (28) for the $m = 0$ mode. A quick check of the remaining values in Table I shows that all but two (marked by an asterisk) are doubly degenerate. It turns out that these two nondegenerate exponents are well described by Eq. (33). (Note that neither of these exponents appear in Figs. 6 and 7, since they are not the exponents of minimum absolute value.) This is demonstrated by Fig. 9, which shows excellent agreement, as a function of α, between this particular subset of the numerical exponents and the analytic result based on the vertical junctions. So Eq. (33) describes some aspects of the dynamics of

TABLE I. The Floquet exponents obtained from a numerical solution of Eqs. (25) and (26) for a periodic ladder with $N=5$, $i_B=10$, $\beta_L=50$, $\beta_c=1$, and $\alpha=0.1$. There are $4*N=20$ characteristic modes of such an array, each mode having a corresponding Floquet exponent. The extremal exponents have values of zero (to a good approximation) and $-1/\beta_c$. All other exponents, except the two marked by an asterisk, are doubly degenerate.

$\mathrm{Re}(\lambda t_c)$
2.6×10^{-4}
-0.01864
-0.01864
-0.04439
-0.04439
-0.16824 (*)
-0.18223
-0.18223
-0.21646
-0.21646
-0.78298
-0.78298
-0.81721
-0.81721
-0.83120 (*)
-0.95505
-0.95505
-0.98080
-0.98080
-0.99969

the array; the decay rates represented in that result, however, merely do not describe the longest-lived mode of the array.

IV. NEAREST-NEIGHBOR MUTUAL INDUCTANCE

A. Numerical results

In this section we study the effects of nearest-neighbor mutual inductance on the stability of phase-locked solutions in *periodic* ladders. Let each loop have a positive self-inductance L as in Sec. III and a negative nearest-neighbor mutual inductance, $-M$, where $M>0$ and $M<L$ [43]. The mesh current analysis of Sec. III can be extended in a straightforward way to handle mutual inductance. In fact, Eqs. (19) and (20) are unchanged. Equation (21), however, must now account for the fact that the total flux through plaquette j depends on the mesh currents I_j and $I_{j\pm1}$:

$$\phi_j-\phi_{j+1}+2\psi_j=-\frac{2\pi}{\Phi_0}(-MI_{j-1}+LI_j-MI_{j+1}). \tag{35}$$

It is useful to introduce a matrix notation to represent the equations compactly. Let $\vec{\phi}$ be an N-component column matrix composed of the ϕ_j. Similarly, let $\vec{\psi}$ represent the phase differences across the vertical junctions, and $\vec{I}$ represents the N mesh currents. Equation (35) can now be written as

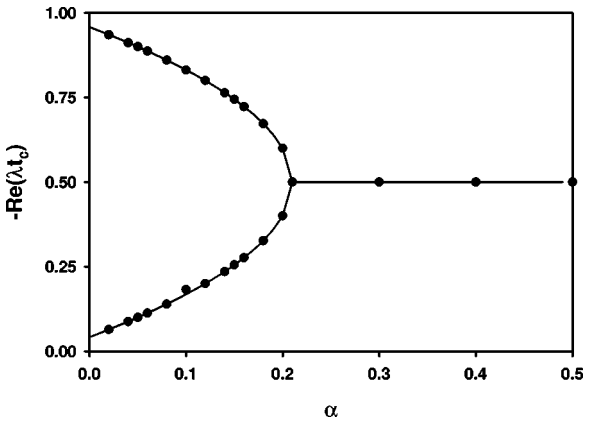

FIG. 9. Agreement between two (out of the set of $4N$) numerical Floquet exponents for a five-cell periodic ladder and an analytic result (solid line) for the exponents based on the *vertical* junctions [Eq. (33)]. This plot demonstrates that the vertical junctions are responsible for some of the stability of the ladder. These results correspond to $i_B=10$, $\beta_L=50$ and $\beta_c=1$.

$$\hat{Z}\cdot\vec{\phi}+2\vec{\psi}=-\frac{2\pi}{\Phi_0}\hat{L}\cdot\vec{I}, \tag{36}$$

where $\hat{Z}$ and $\hat{L}$ are $N\times N$ matrices, the forms of which can be deduced from Eq. (35). Note that $\hat{L}$ is just the inductance matrix with the self-inductance L along the diagonal, and the mutual inductance $-M$ on either side of the diagonal (along with the constraint of periodic boundary conditions).

We can write Eq. (36) in a dimensionless form as follows. Factor out L from the inductance matrix, and define a dimensionless mutual inductance $\mu_L\equiv M/L$. Then write $\hat{L}=L\hat{X}$ and we now have

$$\hat{Z}\cdot\vec{\phi}+2\vec{\psi}=-\frac{2\pi L}{\Phi_0}\hat{X}\cdot\vec{I}.$$

Define the dimensionless mesh current matrix $\vec{i}\equiv\vec{I}/I_{cx}$. Then

$$\hat{Z}\cdot\vec{\phi}+2\vec{\psi}=-\frac{2\pi LI_{cx}}{\Phi_0}\hat{X}\cdot\vec{i}=-\beta_L\hat{X}\cdot\vec{i}. \tag{37}$$

We can also write Eqs. (19) and (20) in matrix form. Define $\vec{i}_B\equiv\vec{I}_B/I_{cx}$ to be the dimensionless bias current matrix, and let $\sin\vec{\phi}$ ($\sin\vec{\psi}$) be the notation denoting the matrix whose elements are $\sin\phi_j$($\sin\psi_j$). Then we have

$$\vec{i}_B+\hat{Z}^{\mathrm{Tr}}\cdot\vec{i}-\sin\vec{\phi}-\frac{d\vec{\phi}}{d\tau}-\beta_c\frac{d^2\vec{\phi}}{d\tau^2}=0, \tag{38}$$

$$\vec{i}-\alpha\sin\vec{\psi}-\frac{d\vec{\psi}}{d\tau}-\beta_c\frac{d^2\vec{\psi}}{d\tau^2}=0, \tag{39}$$

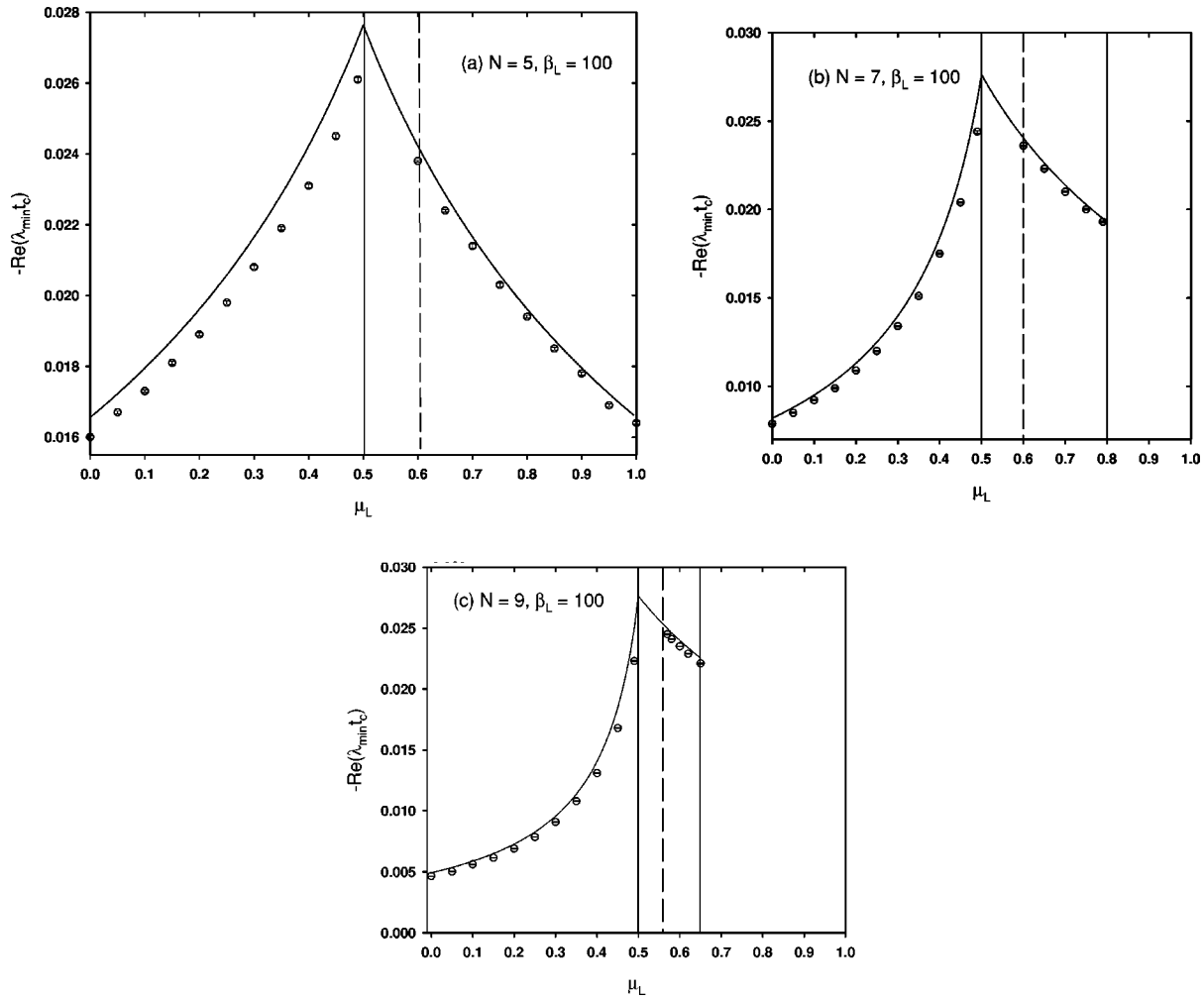

FIG. 10. Minimum Floquet exponent for periodic ladders vs the dimensionless, nearest-neighbor mutual inductance. (The results correspond to $i_B=10$, $\beta_c=10$, and $\beta_L=100$.) The symbols correspond to exponents, for a given value of μ_L, that were averaged over many different values of the run time of the code as well as several different random configurations of initial voltages. The error bars represent the standard deviation of the average exponent. The solid line represents an analytic result [Eq. (45)] based on a DSG equation for the horizontal junctions. (a) $N=5$. The analytic result predicts stable phase-locked solutions for $0\leqslant\mu_L\leqslant 1$. The numerical results exhibit an instability, however, for $\mu_L^{(1)}\leqslant\mu_L\leqslant\mu_L^{(2)}$ where $\mu_L^{(1)}=0.5$ (solid vertical line) and $\mu_L^{(2)}$ (dotted vertical line) is dependent on the starting configuration of phases and voltages, as well as on the value of β_L. This instability originates with the vertical junctions. (b) $N=7$. In this case, the geometry of the ladder leads to a second instability region for $\mu_L>0.8$ (marked by a solid vertical line) that originates with the horizontal junctions. The instability near $\mu_L=0.5$ still exists but is narrower than for the five-cell ladder. (c) $N=9$. The instability due to the horizontal junctions exists for $\mu_L>0.67$. The instability near $\mu_L=0.5$ is also still present.

where $\hat{Z}^{\mathrm{Tr}}$ is the transpose of $\hat{Z}$. As in Sec. III we can eliminate the mesh current from Eqs. (38) and (39). Solve Eq. (37) for $\vec{i}$ and substitute into Eqs. (38) and (39). The result is

$$\beta_c\frac{d^2\vec{\phi}}{d\tau^2}+\frac{d\vec{\phi}}{d\tau}+\sin\vec{\phi}+\frac{1}{\beta_L}\hat{Z}^{\mathrm{Tr}}\cdot\hat{X}^{-1}\cdot(\hat{Z}\cdot\vec{\phi}+2\vec{\psi})-i_B=0, \tag{40}$$

$$\beta_c\frac{d^2\vec{\psi}}{d\tau^2}+\frac{d\vec{\psi}}{d\tau}+\alpha\sin\vec{\psi}+\frac{1}{\beta_L}\hat{X}^{-1}\cdot(\hat{Z}\cdot\vec{\phi}+2\vec{\psi})=0. \tag{41}$$

Equations (40) and (41) were solved numerically for $\vec{\phi}$ and $\vec{\psi}$ as a function of time for random initial values of $d\vec{\phi}/d\tau$ and $d\vec{\psi}/d\tau$ and initial values of $\vec{\phi}$ and $\vec{\psi}$ of zero.

A stability analysis analogous to that in Sec. III yields

$$\beta_c\frac{d^2\vec{\eta}}{d\tau^2}+\frac{d\vec{\eta}}{d\tau}+\cos\vec{\phi}_0\cdot\vec{\eta}+\frac{1}{\beta_L}\hat{Z}^{\mathrm{Tr}}\cdot\hat{X}^{-1}\cdot(\hat{Z}\cdot\vec{\eta}+2\vec{\delta})=0, \tag{42}$$

$$\beta_c\frac{d^2\vec{\delta}}{d\tau^2}+\frac{d\vec{\delta}}{d\tau}+\alpha\cos\vec{\psi}_0\cdot\vec{\delta}+\frac{1}{\beta_L}\hat{X}^{-1}\cdot(\hat{Z}\cdot\vec{\eta}+2\vec{\delta})=0. \tag{43}$$

Equations (40)–(43) allow a numerical calculation of the Floquet exponents as functions of N, i_B, β_c, β_L, and μ_L.

Figure 10(a) shows the minimum Floquet exponent as a function of μ_L for $0 \leqslant \mu_L \leqslant 1$ for a five-cell periodic ladder. As a theoretical exploration of the behavior of the RCSJ equations we are content to allow μ_L to vary over this range. Physically, we know that in a simple ladder array with only nearest-neighbor mutual inductance, the maximum value of this ratio is one-half [43]. It may be of interest for experimentalists to attempt ways to enhance the mutual inductance over the self-inductance in order to see if a broader range of μ_L values can be sampled.

The small error bars visible in Fig. 10 deserve explanation. In order to produce plots that displayed an interesting dependence of the Floquet exponents on the mutual inductance, we found a rather large value of β_L was necessary ($\beta_L = 100$). A consequence of such a large self-inductance, we also found, was some small dependence of the numerically calculated exponents on the run time of the code as well as the values of the initial voltages across the horizontal junctions. We therefore calculated, for each different value of the mutual inductance μ_L, the exponents for many different values of the run time and several different random configurations of initial voltages. The symbols in Fig. 10 represent an average, for a given value of μ_L, over these sets of results, and the error bars represent the standard deviation of the average. The relatively small size of the error bars shows that the variations in the numerically calculated exponents is small. The behavior has been discussed elsewhere [47].

In Fig. 10(a), which corresponds to a periodic ladder with $N=5$, we checked that the data for $\mu_L = 0$ are to a good approximation given by Eq. (28), as expected. Interestingly, then, as μ_L is increased from zero towards 0.5, the stability of phase locking increases, while it decreases for increasing μ_L greater than approximately 0.6. Even more interesting is the behavior of the ladder in the range $0.5 \leqslant \mu_L \leqslant 0.6$. For these values of the mutual inductance the ladder is actually unstable. This is evidenced by very rapidly growing phases, voltages, and mesh currents with time as Eqs. (40) and (41) are numerically integrated. For $N=5$, the lower limit of this instability region is $\mu_L^{(1)} = 0.5$ independent of other circuit parameters such as β_c and β_L. The upper limit of this region, which we denote by $\mu_L^{(2)}$, depends on such quantities as the value of the starting voltages as well as on the value of β_L. For example, for a fixed set of starting voltages, we find that $\mu_L^{(2)}$ is a decreasing function of β_L, as shown in Fig. 11. Also, it is interesting to note that this instability region does not appear at all if both the phases *and* the voltages are initialized to zero. (See discussion below for the reason for this behavior.)

Physically, it appears that this instability is due to competition between the self-inductance of a given loop (say, loop j), which wishes to have a mesh current with a given sense of circulation, and the mutual inductance of the two neighboring loops ($j \pm 1$), which wish to have the mesh current in loop j flow in the opposite sense. Figure 12 shows the spatially averaged mesh currents for a five-cell ladder as a function of μ_L for $\beta_c = 10$ and $\beta_L = 100$. The values were produced by integrating Eqs. (40) and (41) for 10^6 time steps and recording the ending value of the mesh currents based as on the matrix equation

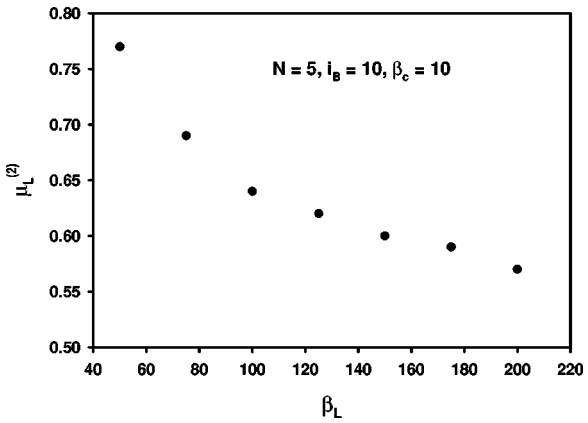

FIG. 11. Evidence that the upper boundary, $\mu_L^{(2)}$, of the instability region due to the vertical junctions is a function of the loop self-inductance, β_L. The value of $\mu_L^{(2)}$ was determined by finding, for a fixed starting configuration of voltages and phase differences, that largest value of the mutual inductance that resulted in an exponential growth of the phases and voltages.

$$\vec{i} = -\frac{1}{\beta_L}\hat{X}^{-1}\cdot(\hat{Z}\cdot\vec{\phi} + 2\vec{\psi}). \tag{44}$$

Note that the mesh currents switch sense of circulation (as represented by the sign change) as μ_L is increased. In the instability region the mesh currents essentially diverge as the equations are integrated numerically, and just before the instability is reached, for $0.45 \leqslant \mu_L \leqslant 0.49$, the mesh currents are zero. This instability in the vicinity of $\mu_L = 0.5$ also occurs for periodic ladders with $N=6$, 7, 8, and 9, all the lad-

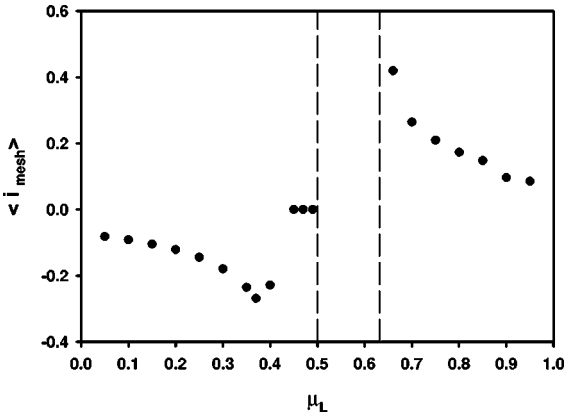

FIG. 12. Spatially averaged *mesh* currents vs the dimensionless nearest-neighbor mutual inductance for $N=5$ in a periodic ladder. (The results correspond to $\beta_c = 10$, $\beta_L = 100$.) These quantities were obtained by starting with a random configuration of phases and voltages and numerically integrating Eqs. (40) and (41) for a long time. Each of the five mesh currents were calculated from Eq. (44) at the end of this time, and then the five values were arithmetically averaged. All results shown in the figure were obtained by initializing to the same set of random phases and voltages.

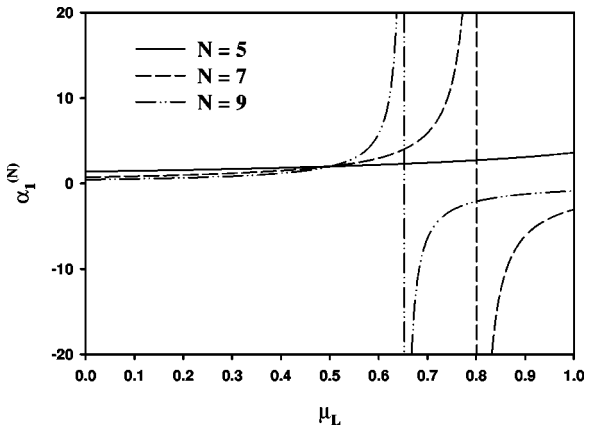

FIG. 13. Plot of the function $\alpha_1^{(N)}$, the effective normal-mode frequency of the inductively coupled horizontal junctions, versus the dimensionless nearest-neighbor mutual inductance for three different sized ladders with periodic boundary conditions. Unstable phase-locked solutions occur if $\alpha_1^{(N)}$ is negative.

ders we have in fact studied. Indeed, one would expect this competition-induced instability to be independent of ladder size for the case of nearest-neighbor mutual inductance in that the onset of the instability should always occur at $\mu_L = 0.5$.

Although, as mentioned above, the seven-cell and nine-cell ladders exhibit the instability near $\mu_L = 0.5$ just like $N = 5$ [see Figs. 10(b) and 10(c)], they both also have a *second* instability region that the five-cell ladder does not exhibit. These second instability regions have an onset at a value of $\mu_L^{(3)} > \mu_L^{(2)}$ that is dependent on ladder size. These new instability regions extend up to $\mu_L = 1$ and are marked by a vertical line at the value of $\mu_L^{(3)}$. We now turn to an analytic calculation of the Floquet exponents, which helps us understand the source of these instabilities.

B. Analytical results

We proceed basically the same as for the case of the self-inductive ladder with periodic boundary conditions, except now we have matrices to manipulate. We start with Eq. (42) and ignore the effects of the vertical junctions, i.e., let $\vec{\delta} \to 0$. The results for the Floquet exponents in that case are

$$\mathrm{Re}(\lambda_m^{(M)} t_c) = -\frac{1}{2\beta_c} \pm \frac{1}{2\beta_c} \mathrm{Re}\sqrt{1 - 4\alpha_m^{(N)}\left(\frac{\beta_c}{\beta_L}\right)}. \quad (45)$$

where we can think of the $\alpha_m^{(N)}$ as *effective* normal-mode frequencies of the inductively coupled horizontal junctions. We find

$$\alpha_m^{(5)} = \frac{1}{(\mu_L^2 - \mu_L - 1)}\left[-2 + 2(1-\mu_L)\cos\left(\frac{2\pi m}{N}\right) + 2\mu_L \cos\left(\frac{4\pi m}{N}\right)\right], \quad (46)$$

$$\alpha_m^{(7)} = \frac{2(\mu_L^2 - 1) - 2(\mu_L^2 + \mu_L - 1)\cos\left(\frac{2\pi m}{N}\right) - 2\mu_L(\mu_L - 1)\cos\left(\frac{4\pi m}{N}\right) + 2\mu_L^2 \cos\left(\frac{6\pi m}{N}\right)}{\mu_L^3 + 2\mu_L^2 - \mu_L - 1}, \quad (47)$$

and

$$\alpha_m^{(9)} = \frac{2(1-2\mu_L^2) - 2(\mu_L^3 - 2\mu_L^2 - \mu_L + 1)\cos\left(\frac{2\pi m}{N}\right) + 2\mu_L(\mu_L^2 + \mu_L - 1)\cos\left(\frac{4\pi m}{N}\right)}{\mu_L^4 - 2\mu_L^3 - 3\mu_L^2 + \mu_L + 1} + \frac{2\mu_L^2(\mu_l - 1)\cos\left(\frac{6\pi m}{N}\right) - 2\mu_L^3 \cos\left(\frac{8\pi m}{N}\right)}{\mu_L^4 - 2\mu_L^3 - 3\mu_L^2 + \mu_L + 1}. \quad (48)$$

These analytic results were used to produce the solid curves in Figs. 10(a), 10(b), and 10(c).

In contrast to Sec. III where only loop self-inductance was included, the argument inside the square root of Eq. (45) could, for particular values of m, $\alpha_m^{(N)}$, β_c and β_L, be positive and larger than one. If this happens, at least one of the Floquet exponents will be positive, signaling unstable phase-locked solutions. In fact, such an instability will occur if $\alpha_m^{(N)}(\mu_L) < 0$ for any values of μ_L, that is, when an *effective* normal-mode frequency goes negative. Plots of $\alpha_1^{(N)}$ vs μ_L for $N = 5$, 7, and 9 are shown in Fig. 13. We now see the reason for the second instability region in the seven- and nine-cell ladders; the $m = 1$ normal-mode frequency has indeed gone negative. We have checked that $\alpha_0^{(N)} = 0$ and $\alpha_m^{(N)} > 0$ for $m \neq 1$ for $N = 5$, 7, and 9. Also notice that $\alpha_1^{(5)} > 0$ for $0 \leqslant \mu_L \leqslant 1$. Figure 13 does not, however, explain the

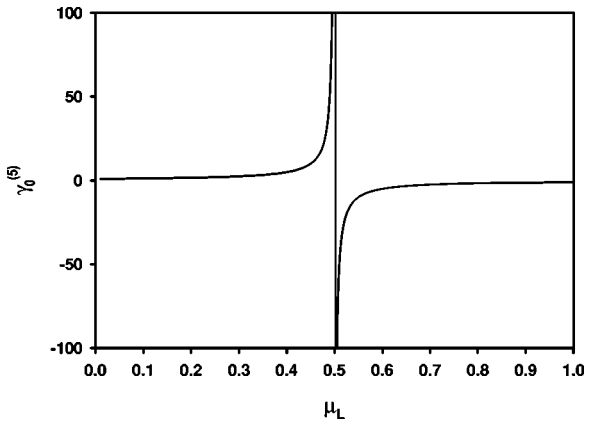

FIG. 14. A plot of the geometry-dependent function $\gamma_0^{(5)}$ vs the dimensionless nearest-neighbor mutual inductance for a ladder with $N=5$ and periodic boundary conditions. This function conveys information about the stability of the *vertical* junctions [Eq. (49)]. A solution for the phase differences across the vertical junctions that exponentially grows with time occurs if $\gamma_m^{(5)}<-\alpha\beta_L\cos\psi_0/2$ for any m. If we assume that $\cos\psi_0>0$, then we expect an instability for a range of values of μ_L that causes $\gamma_m^{(5)}$ to be negative and to satisfy this inequality.

instability near $\mu_L=0.5$, because $\alpha_m^{(N)}$ is clearly positive in this region. For an appreciation of the cause of this instability we must look at the behavior of the vertical junctions.

We return to Eq. (43), let $\vec{\eta}=0$ and calculate a set of effective Floquet exponents for the vertical junctions:

$$\Lambda_m^{(M)}t_c=-\frac{1}{2\beta_c}\pm\frac{1}{2\beta_c}\sqrt{1-4\beta_c\left[\alpha\cos\psi_0+\frac{2\gamma_m^{(N)}}{\beta_L}\right]}, \tag{49}$$

where, for $N=5$, the geometric factor $\gamma_m^{(N)}$ is

$$\gamma_m^{(5)}=\frac{\mu_L^4-3\mu_L^2+1}{1-5\mu_L^2+5\mu_L^4-2\mu_L^5}+\frac{2\mu_L(1-\mu_L)\cos\left(\frac{2\pi m}{N}\right)+2\mu_L^2\cos\left(\frac{4\pi m}{N}\right)}{2\mu_L^3-3\mu_L^2-\mu_L+1}. \tag{50}$$

In this case, the vertical junctions will exhibit an exponentially growing phase difference if

$$\gamma_m^{(N)}<-\frac{\alpha\beta_L\cos\psi_0}{2}. \tag{51}$$

Now a plot of $\gamma_0^{(5)}$ vs μ_L is shown in Fig. 14. We see that the function abruptly becomes negative at $\mu_L=0.5$. (We have checked that $\gamma_m^{(5)}>0$ for $m\neq 0$. Also, we see similar behavior for the seven- and nine-cell ladders.) If we assume that $\cos\psi_0>0$, then the vertical junctions will be unstable for $\gamma_m^{(N)}<0$. Based on Fig. 14 for $N=5$ we see then that an instability region will exist for a range of μ_L values, $\mu_L^{(1)}\leqslant\mu_L\leqslant\mu_L^{(2)}$ where it is clear that $\mu_L^{(1)}=0.5$. Then, based on Eq. (51) and Fig. 14, we see that the value of $\mu_L^{(2)}$ will depend on the value of α, β_L, and $\cos\psi_0$. For example, as β_L increases we expect that $\mu_L^{(2)}$ will decrease, i.e., approach a value of 0.5. This conclusion is indeed in accordance with the behavior of the numerical exponents, as shown in Fig. 11. Also, Eq. (51) suggests that the value of $\mu_L^{(2)}$ should also depend on the value of $\cos\psi_0$. This is relevant to the numerical results in Fig. 10, where we explained that the upper boundary of the instability region near $\mu_L=0.5$ depends on the choice of the starting configuration of phases and voltages. In general, then, it is clear that the instability near $\mu_L=0.5$ originates with the *vertical* junctions and would thus be missed by an analysis that was based on a DSG equation for the horizontal phase differences. It is also clear why this instability does not appear numerically when *both* the Josephson phases and the voltages across the junctions are initialized to zero. In such a scenario, although the horizontal junctions will be active, the only possible solution for the vertical junctions is to keep zero voltages and Josephson phases for all times. Since we know this instability is triggered by the vertical junctions, the vertical junctions have no change to ''go unstable'' and thus instability never appears.

V. LONG-RANGE INTERACTIONS

A. Numerical results

To allow for mutual inductances of extended range in a periodic ladder, we assume an inductance matrix of the following form:

$$L_{jk}=\begin{cases}L & j=k\\ -M & j=k\pm1\\ -Me^{-s|j-k|} & \text{otherwise.}\end{cases} \tag{52}$$

The formalism of Sec. IV can be applied to this case with the only change being the use of the full inductance matrix. Note that s controls the range of the inductance. For $s\to 0$, we have ''infinite-range'' inductance, meaning that the mutual inductance between cells j and $k(j\neq k)$ is $-M$ for all k. For $s\to\infty$ we return to the case of only nearest-neighbor mutual inductances. For $0<s<\infty$, the inductance has a value of $-M$ for nearest-neighbor cells and then falls off exponentially with distance for more distant cells.

Our numerical results for the Floquet exponents as a function of μ_L for a five-cell periodic ladder are shown in Fig. 15. All exponents were calculated for the same random starting configuration of voltages, while all phases were initialized to zero. A range of s values was studied. Note that the inclusion of long-range inductance has not removed the instability that was apparent in the nearest-neighbor case. This is noticeable in the figure by a gap in the numerical results for a range of μ_L values. Observation also shows that the exponents for $s=10$ in the figure are essentially the same as those in Fig. 10(a), which would correspond to $s\to\infty$. The

range of inductances over which the instability occurs, $\mu_L^{(1)} \leqslant \mu_L \leqslant \mu_L^{(2)}$, is dependent on s. As we decrease s from $s=10$ to $s=0$, thereby *increasing* the effective range of the mutual inductance, the value of $\mu_L^{(1)}$ shifts from $\mu_L^{(1)}=0.5$ to $\mu_L^{(1)}=0.25$. That is, as the range of the inductance increases $(s \to 0)$, the overall strength M does not have to be as large (compared to case of $s \to \infty$) to cause the instability. Recall that, physically, this instability can be thought of as due to a competition between the mutual and self-inductance in the ladder to configure the mesh currents so as to flow in a particular sense. Also note that for μ_L outside the range $\mu_L^{(1)} \leqslant \mu_L \leqslant \mu_L^{(2)}$ increasing the range of the inductance generally reduces the stability of the phase-locked solutions.

B. Analytical results

Our analysis here is essentially identical to that of the Sec. IV. By neglecting the vertical junctions entirely, we arrive at a version of the DSG equation that includes long-range interactions of the Kac-Baker form [23]. The result for the Floquet exponents is

$$\mathrm{Re}(\lambda_m^{(LR)} t_c) = -\frac{1}{2\beta_c} \pm \frac{1}{2\beta_c}\sqrt{1-4\alpha_m^{(5,LR)}\left(\frac{\beta_c}{\beta_L}\right)}, \quad (53)$$

where

$$\alpha_m^{(5,LR)} \equiv \frac{-2(1+\mu_L e^{-2s})+2[1+\mu_L(2e^{-2s}-1)]\cos\left(\frac{2\pi m}{N}\right)+2[\mu_L-\mu_L e^{-2s}]\cos\left(\frac{4\pi m}{N}\right)}{\mu_L^2(1-3e^{-2s}+e^{-4s})-\mu_L(1+e^{-2s})-1}. \quad (54)$$

Equations (53) and (54) were used to produce the solid curves in Fig. 15. The agreement is quite good, except for the instability regions. As in the previous section, the analytic treatment here is based on a DSG equation that ignores the effects of the vertical junctions. Over much of the region $0 \leqslant \mu_L \leqslant 1$ this approximation works very well, but there are obviously values of the inductance where ignoring the effects of the vertical junctions has catastrophic effects.

VI. CONCLUSIONS

We have studied the stability of phase-locked solutions to ladder arrays of Josephson junctions under both periodic and open boundary conditions and also in the presence of current-induced magnetic fields. We calculate the Floquet exponents numerically, based on the RCSJ model, and also analytically. In the case of zero induced magnetic fields, we calculate the exponents analytically based directly on the RCSJ equations, as well as based on a simplified model of the ladder that leads to a DSG equation for the horizontal junctions only. We find the DSG equation appreciably overestimates the exponents in the overdamped (small β_c regime) due to the neglect of spatial variations in the derivatives of the Josephson phases across the horizontal junctions, $d\phi_j/d\tau$ and $d^2\phi_j/d\tau^2$.

The majority of our analytic work in the case of induced magnetic field effects is limited to a DSG equation for the horizontal junctions. In the case of only self-inductive plaquettes, we find this analytic approach yields good agreement with the numerical exponents for $\beta_c \ll \beta_L$ and $\beta_L \ll \beta_c$. For $\beta_c \approx \beta_L$ the DSG equation differs from the numerical results. Presumably this is from ignoring the effects of the vertical junctions. When mutual inductance is included between plaquettes we find, interestingly, that there are ranges of values of the mutual inductance for which the ladder is unstable. Analytic work, based on a DSG for the horizontal junctions, agrees reasonably well with the numerical results for those values of inductance that yield stable phase locking. However, to understand the cause of all the observed instabilities, it is crucial in the analytic work to consider the behavior of the vertical junctions.

This work has made a comparison of some aspects of the dynamics of two different nonlinear models: the RCSJ model for a ladder geometry, which leads to nonconvex interparticle couplings, and the DSG equation, which has convex inter-

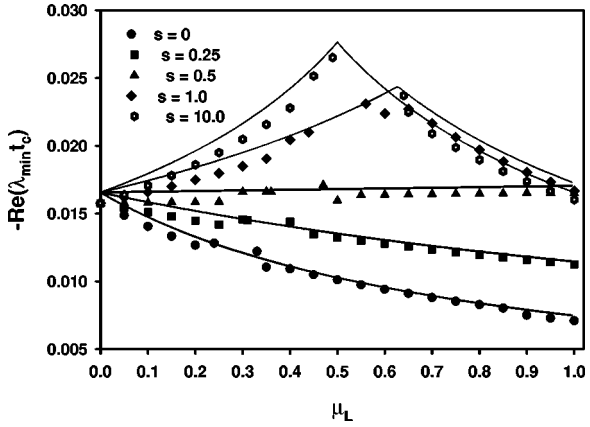

FIG. 15. Minimum Floquet exponents vs the dimensionless mutual inductance for a periodic ladder with $N=5$ and for several different values of the effective range s of the inductance [see Eq. (52)]. (These results correspond to $i_B=10$, $\beta_c=10$, $\beta_L=100$.) $s=0$ corresponds to infinite-range inductance, and $s \to \infty$ corresponds to the limit of only nearest-neighbor inductance. The solid line represents an analytic result [Eq. (53)] based on a DSG equation for the horizontal junctions. The instability that occurs near $\mu_L=0.5$ for $s \to \infty$ still exists for finite s but is shifted to smaller values of μ_L.

particle couplings. We have used Floquet theory as the probe by which these two models have been compared. There is still more analysis that could be performed here, including a more detailed study of the behavior of the Floquet exponents throughout the i_B, β_c, β_L, μ_L, and s parameter space, as well as a comparison of open and periodic boundary conditions for the case of mutually inductive ladders. A more detailed analytic analysis of the behavior of the vertical junctions could also be informative. In general, the more we learn about the dynamics of the ladder array, the better we may also understand more complicated 2D arrays, as the ladder can be thought of as building block of such a larger array.

ACKNOWLEDGMENTS

The authors wish to thank Barbara Andereck, Tom Dillman, Steve Herbert, Mark Jarrell, and David Stroud for useful discussions. This research was funded by the Howard Hughes Medical Institute Undergraduate Biological Sciences Education Program Grant No. 71196-529503 to Ohio Wesleyan University.

[1] P. Caputo, M. V. Fistul, A. V. Ustinov, B. A. Malomed, and S. Flach, Phys. Rev. B **59**, 14 050 (1999).
[2] H. S. J. van der Zant, M. Barahona, A. E. Duwel, E. Trías, T. P. Orlando, S. Watanabe, and S. H. Strogatz, Physica D **119**, 219 (1998).
[3] L. M. Florí, J. L. Marín, S. Aubry, P. J. Martínez, F. Falo, and J. J. Mazo, Physica D **113**, 387 (1998).
[4] M. Barahona, S. H. Strogatz, and T. P. Orlando, Phys. Rev. B **57**, 1181 (1998).
[5] M. Barahona, E. Trías, T. P. Orlando, A. E. Duwel, H. S. J. van der Zant, S. Watanabe, and S. H. Strogatz, Phys. Rev. B **55**, R11 989 (1997).
[6] S. Ryu, W. Yu, and D. Stroud, Phys. Rev. E **53**, 2190 (1996).
[7] C. Denniston and C. Tang, Phys. Rev. Lett. **75**, 3930 (1995).
[8] J. J. Mazo, F. Falo, and L. M. Floría, Phys. Rev. B **52**, 10 433 (1995).
[9] J. M. Kim and S. J. Lee, Phys. Rev. B **50**, 13 829 (1994).
[10] J. Kim, W. G. Choe, S. Kim, and H. J. Lee, Phys. Rev. B **49**, 459 (1994).
[11] P. Binder, D. Abraimov, A. V. Ustinov, S. Flach, and Y. Zolotaryuk, Phys. Rev. Lett. **84**, 745 (2000).
[12] E. Trías, J. J. Mazo, and T. P. Orlando, Phys. Rev. Lett. **84**, 741 (2000).
[13] S. Flach and M. Spicci, J. Phys.: Condens. Matter **11**, 321 (1999).
[14] P. J. Martínez, L. M. Floría, J. L. Marín, S. Aubry, and J. J. Mazo, Physica D **119**, 175 (1998).
[15] L. M. Floría, J. L. Marín, P. J. Martínez, F. Falo, and S. Aubry, Europhys. Lett. **36**, 539 (1996).
[16] P. Barbara, A. B. Cawthorne, S. V. Shitov, and C. J. Lobb, Phys. Rev. Lett. **82**, 1963 (1999).
[17] M. Basler, W. Krech, and K. Yu. Platov, Phys. Rev. B **58**, 3409 (1998).
[18] E. B. Harris and J. C. Garland, Phys. Rev. B **55**, 3832 (1997).
[19] K. Wiesenfeld, S. P. Benz, and P. A. A. Booi, J. Appl. Phys. **76**, 3835 (1994).
[20] M. Kardar, Phys. Rev. B **33**, 3125 (1986).
[21] B. R. Trees and N. Hussain, Phys. Rev. E **61**, 6415 (2000).
[22] L. M. Floría and J. J. Mazo, Adv. Phys. **45**, 505 (1996).
[23] S. F. Mingaleev, Yu. B. Gaididei, E. Majerníková, and S. Shpyrka, Phys. Rev. E **61**, 4454 (2000), and references therein.
[24] S. N. Coppersmith and D. S. Fisher, Phys. Rev. B **28**, 2566 (1983), and references therein.
[25] Two review articles on the dynamics of the F-K model are: Ref. [15] and O. M. Braun and Yu. S. Kivshar, Phys. Rep. **306**, 1 (1998).
[26] Z. Q. Wang and D. Stroud, Phys. Rev. B **44**, 9643 (1991).
[27] It is already known that the ground states of the two models are equivalent. K. Sasaki and R. B. Griffiths, J. Stat. Phys. **53**, 1031 (1988).
[28] A. V. Ustinov, M. Cirillo, and B. A. Malomed, Phys. Rev. B **47**, 8357 (1993).
[29] H. S. J. van der Zant, T. P. Orlando, S. Watanabe, and S. H. Strogatz, Phys. Rev. Lett. **74**, 174 (1995).
[30] S. Watanabe, S. H. Strogatz, H. S. J. van der Zant, and T. P. Orlando, Phys. Rev. Lett. **74**, 379 (1995).
[31] S. Watanabe, H. S. J. van der Zant, S. H. Strogatz, and T. P. Orlando, Physica D **97**, 429 (1996).
[32] See Figs. 7 and 9 in Ref. [21]. An error in the code that produced the numerical exponents for the ladder based on the RCSJ model has since been identified and corrected. The ladder data in Fig. 7 in Ref. [21] are not qualitatively changed by the correction, but the $N=10$ data, for example, are approximately uniformly increased by a factor of about 1.4 in the *overdamped* regime. The underdamped regime still follows the expected $-1/2\beta_c$ behavior as seen in Fig. 7 of Ref. [21]. See Figs. 2(a) and 3(a) in the present paper for the corrected numerical results.
[33] E. E. Trías, J. J. Mazo, F. Falo, and T. P. Orlando, Phys. Rev. E **61**, 2257 (2000).
[34] D. W. Jordan and P. Smith, *Nonlinear Ordinary Differential Equations* (Clarendon, Oxford, 1977).
[35] If *any* exponents are positive, then phase locking in the ladder, for the given values of bias current, capacitance, and critical current anisotropy, is not stable because perturbations grow with time.
[36] G. Filatrella and K. Wiesenfeld, J. Appl. Phys. **78**, 1878 (1995).
[37] M. Tinkham, *Introduction to Superconductivity* (McGraw-Hill, New York, 1996).
[38] It should be noted that the equivalent structure of Eqs. (10) and (14) is merely a reflection of the mathematical structure underlying Eq. (1). See A. E. Miroshnichenko, S. Flach, M. V. Fistul, Y. Zolotaryuk, and J. B. Page, arXiv:cond-mat/0103280.
[39] G. Grimaldí, G. Filatrella, S. Pace, and U. Gambardella, Phys. Lett. A **223**, 463 (1996).
[40] J. J. Mazo and J. C. Ciria, Phys. Rev. B **54**, 16 068 (1996).

[41] D. Domínguez and J. V. José, Phys. Rev. B **53**, 11 692 (1996).
[42] R. D. Bock, J. R. Phillips, H. S. J. van der Zant, and T. P. Orlando, Phys. Rev. B **49**, 10 009 (1994).
[43] J. R. Phillips, H. S. J. van der Zant, J. White, and T. P. Orlando, Phys. Rev. B **47**, 5219 (1993).
[44] A. Majhofer, T. Wolf, and W. Dieterich, Phys. Rev. B **44**, 9634 (1991).
[45] D. Domínguez and J. V. José, Phys. Rev. Lett. **69**, 514 (1992).
[46] J. W. Nilsson and S. A. Riedel, *Electric Circuits* (Addison-Wesley, Reading, MA, 1996).
[47] B. R. Trees and R. A. Murgescu, Phys. Rev. B **63**, 144503 (2001).